Electronic Supplementary Material (ESI) for Analyst.

Supporting Information

Sensitively detecting endogenous homocysteine in human serum and cardiomyocytes with a specific fluorescent probe

Huan Li[a], Qiwei Wang[a], Lili Shi[b]*, and Tao Li[a]*

[a] Department of Chemistry, University of Science and Technology of China, 96 Jinzhai Road, Hefei, Anhui 230026, China

[b] Department of Chemistry, Anhui University, 111 Jiulong Road, Hefei, Anhui 230601, China.

[a*] E-mail: tlitao@ustc.edu.cn

[b*] E-mail: llshi@ustc.edu.cn

Table of contents:

1. Experimental Section

Synthesis of $PyNTs_3$. In a 50 mL round-bottom three-necked flask containing 4-Methyl-N,N-bis(2-(4-methylphenylsulfonamido)ethyl)benzenesulfonamide (0.226 g, 0.4 mmol) and cesium carbonate (0.2736 g, 1.03 mmol) was added acetonitrile (9.6 mL), and heated the mixture to reflux (100 °C), a acetonitrile (4 mL) solution of 2, 6-dimethyl (bromo-pyridine) (0.106 g, 0.4 mmol) was then slowly dropped. The mixture was stirred overnight under reflux conditions. After the reaction was over, cooled to room temperature. After filtration, a rotary evaporator was used to remove the solvent to obtain the crude product. The product was then purified by silica-gel column chromatography (ethyl acetate: petroleum ether = 50:50, v/v). Light yellow solid (0.236g, 88%) was obtained. ^{1}H NMR (400 MHz, $CDCl_3$) δ = 7.75 (t, J = 7.6 Hz, 1H), 7.72 (d, J = 7.6 Hz, 4H), 7.65 (d, J = 7.6 Hz, 2H), 7.43 (d, J = 7.4 Hz, 2H), 7.34 (d, J = 7.4 Hz, 4H), 7.27 (d, J = 7.4 Hz, 2H), 4.29 (bs, 4H), 3.32 (t, J = 7.4 Hz, 4H), 2.75 (bs, 4H), 2.45 (s, 6H), 2.41 (s, 3H). MS(ESI): m/z $[M + H]^+$ = calcd. for $C_{32}H_{37}N_4O_6S_3^+$ 669.1870; found 669.1865.

Synthesis of $PyNH_3$. To a 10 mL round-bottom flask containing the above product $PyNTs_3$ (0.067 g, 0.1mmol) was added concentrated sulfuric acid (2 mL) at room temperature, and the reaction mixture was stirred at 160 °C in an oil bath for 30 min. After the reaction was over, it was cooled to room temperature and ice water (5 mL) was added before adding 30% NaOH aqueous solution. CH_2Cl_2 (3x50 mL) was used for extraction, and the organic phase was dried with anhydrous Na_2SO_4. After filtration, a rotary evaporator was used to remove the solvent to obtain a yellow oil product. No further purification was required for the next step. The yield of the reaction ranged from 55% to 80%. ^{1}H NMR (400 MHz, $CDCl_3$) δ = 7.52 (t, J = 7.5Hz, 1H), 7.00 (d, J = 7.5 Hz, 2H), 3.96 (s, 4H), 2.71(s, 4H), 2.4 (s, 4H). MS (ESI): m/z $[M + H]^+$ = calcd. for $C_{11}H_9N_4^+$ 207.1604; found 207.1611.

Synthesis of Coumarin-N. To a 50 mL round-bottom three-necked flask containing 4-Chloro-7-nitro-2,1,3-benzoxadiazole (0.025 g, 0.1 mmol) and $PyNH_3$ (0.062 g, 0.3 mmol) was added 20 mL acetonitrile. The resulting mixture reacted at room temperature for 3 hours. Then sodium triacethoxyborohydride (0.085 g, 0.4 mmol) was added and reacted for 4 hours. After the reaction was complete, sodium bicarbonate was added to quench, CH_2Cl_2 (3x50 mL) was extracted, and the organic phase was dried with anhydrous Na_2SO_4. After filtration, the solvent was removed under pressure to obtain solid crude products. The yellow solid (0.035 g, 81%) was obtained by washing with methanol several times and finally vacuum drying. ^{1}H NMR (400 MHz,

DMSO) δ = 7.70 (d, J = 8.50 Hz, H), 8.51 (d, J = 7.59 Hz, H), 7.13 (m, J = 8.6 Hz, 3H), 6.54 (J = 1.45 Hz, H), 3.87 (m, 6H), 2.87 (m, J = 7.2Hz, 4H), 2.57 (m, J = 1.37 Hz, 6H),2.37 (d, J = 7.2 Hz, 2H), 1.15 (t, J = 7.02 Hz, 4H). MS (ESI): m/z $[M + H]^+$ = calcd. for $C_{25}H_{34}N_5O_2^+$ 436.2707; found 436.2834.

Synthesis of NBD-NH_2-DPA. To a 50 mL round-bottom three-necked flask containing 4-Chloro-7-(diethylamino)-2-oxo-2H-chromene-3-carbaldehyde (0.019 g, 0.1 mmol) and triethylamine (0.014 mL, 0.1 mmol) was added 20 mL $CHCl_3$. (N1, N1-Bis(pyridin-2-ylmethyl)ethane-1,2-diamine) (0.073g, 0.3 mmol) was then added to the reaction mixture. The resulting mixture was heated to 60 °C and stirred in N_2 for 4 h. After the reaction was over, it was cooled to room temperature and evaporated to a solid. Then dissolved in CH_2Cl_2, the impurities were extracted using NaOH and ice deionized water. The organic layer was combined, dried over anhydrous sodium sulfate, and then concentrated with a rotary evaporator to obtain a solid crude product. The product was then purified by silica-gel column chromatography (chloroform: methanol = 10:1, v/v). Dark orange solid (0.016g, 40.7%) was obtained. ^{1}H NMR (400 MHz, DMSO) δ = 2.74 (t, J = 2.7 Hz, 2H), 2.85 (t, J = 2.7 Hz, 2H), 3.87 (s, 4H), 7.25 (d, J = 2.7 Hz, H), 7.45-7.74 (ddd, J = 2.7 Hz, 4H), 7.75 (ddd, J = 7.5 Hz, 2H), 8.51 (d, 2H). MS (ESI): m/z $[M + H]^+$ = calcd. for $C_{20}H_{20}N_7O_3^+$ 406.1622; found 406.1631.

Synthesis of Coumarin-NH_2-DPA. To a 25 mL round-bottom three-necked flask containing 4-Chloro-7-nitro-2,1,3-benzoxadiazole (0.025 g, 0.1 mmol) and (N1, N1-Bis(pyridin-2-ylmethyl)ethane-1,2-diamine) (0.024 g, 0.1 mmol) was added anhydrous DMF (5 mL). Potassium carbonate (0.028 g, 0.2 mmol) was then added to the reaction mixture. The resulting mixture was heated at 80 °C and stirred for 30 min. After the reaction was over, it was cooled to room temperature and the products were precipitated with ice ether, filtered, and washed with ether several times to obtain a solid crude. After washing with methanol several times and vacuum drying, the product was dark purple (0.029 g, 61%). ^{1}H NMR (400 MHz, DMSO) δ = 10.05 (s, H), 8.51 (d, J = 8.6 Hz, H), 7.74-7.66 (J = 8.6 Hz, 3H), 7.31-7.24 (J = 7.2 Hz, 4H), 6.69 (d, J = 7.2 Hz, 1H), 6.49 (d, J = 7.2 Hz, 1H), 3.94 (J = 1.37 Hz, 4H), 2.75-2.90 (J = 7.2 Hz, 6H), 2.50 (t, J = 4.7 Hz, 1H), 1.10 (t, J = 7.2 Hz, 6H). MS (ESI): m/z $[M + H]^+$ = calcd. for $C_{28}H_{32}N_5O_3^+$ 486.2500; found 486.2499.

2. Supplementary Figures and Discussions

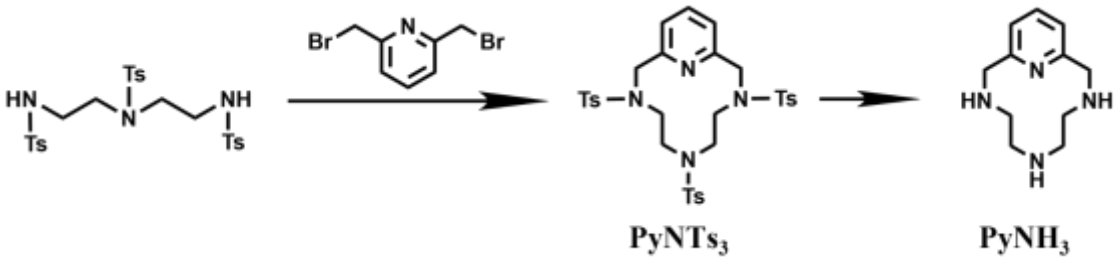

Figure S1. The synthetic routes of raw materials.

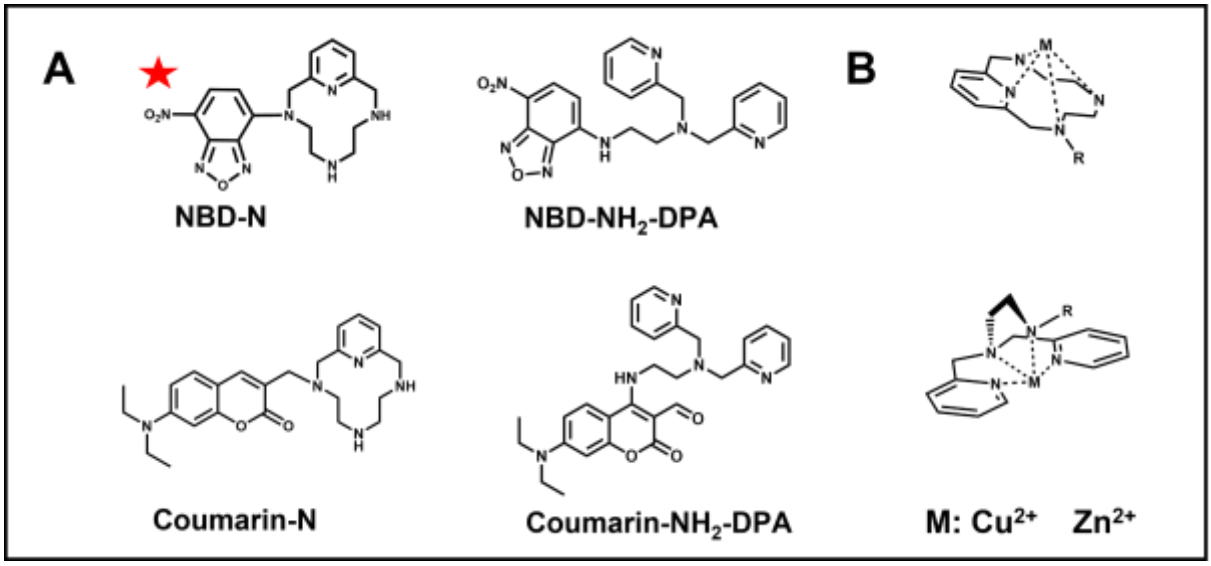

Figure S2. The structure of four probes (A) and complexation modes with metal ions (B).

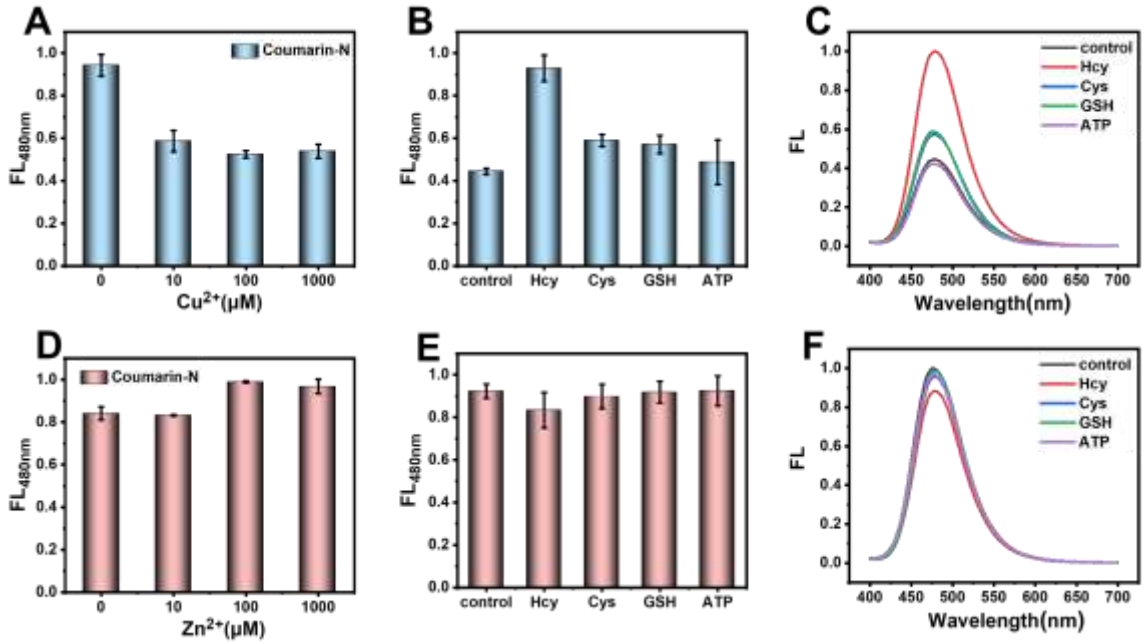

Figure S3. Detection effect of Coumarin-N after complexing with metal ions. (A) Fluorescence changes of Coumarin-N after interaction with different concentrations of Cu^{2+}. (B)Fluorescence intensity of Coumarin-N-Cu^{2+} toward various analytes. (C) Fluorescence spectra of Coumarin-N-Cu^{2+} toward various analytes. (D) Fluorescence changes of Coumarin-N after interaction with different concentrations of Zn^{2+}. (E) Fluorescence intensity of Coumarin-N-Zn^{2+} toward various analytes. (F) Fluorescence spectra of Coumarin-N-Zn^{2+} toward various analytes.

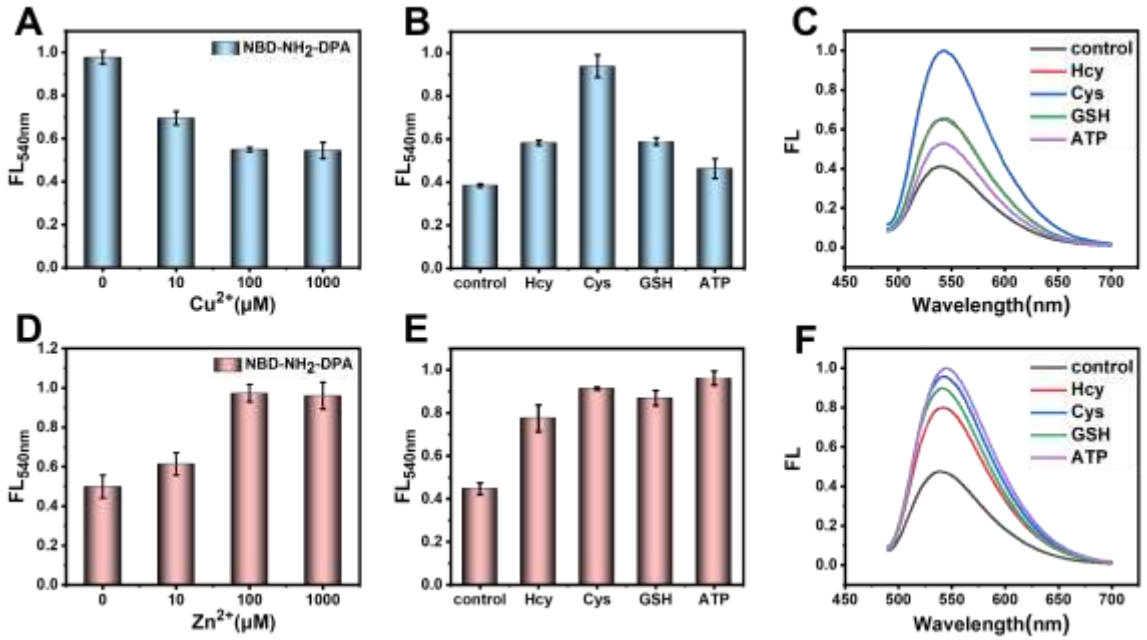

Figure S4. Detection effect of NBD-NH_2-DPA after complexing with metal ions. (A) Fluorescence changes of NBD-NH_2-DPA after interaction with different concentrations of Cu^{2+}. (B)Fluorescence intensity of NBD-NH_2-DPA-Cu^{2+} toward various analytes. (C) Fluorescence spectra of NBD-NH_2-DPA-Cu^{2+} toward various analytes. (D) Fluorescence changes of NBD-NH_2-DPA after interaction with different concentrations of Zn^{2+}. (E) Fluorescence intensity of NBD-NH_2-DPA-Zn^{2+} toward various analytes. (F) Fluorescence spectra of NBD-NH_2-DPA-Zn^{2+} toward various analytes.

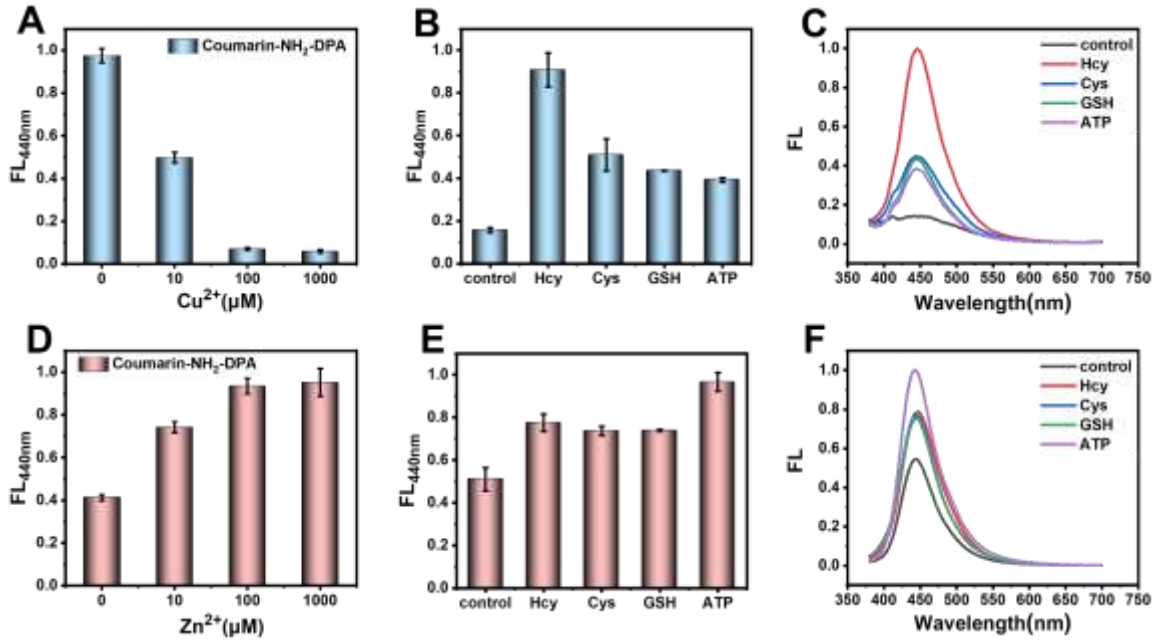

Figure S5. Detection effect of Coumarin-NH_2-DPA after complexing with metal ions. (A) Fluorescence changes of Coumarin-NH_2-DPA after interaction with different concentrations of Cu^{2+}. (B)Fluorescence intensity of Coumarin-NH_2-DPA-Cu^{2+} toward various analytes. (C) Fluorescence spectra of Coumarin-NH_2-DPA-Cu^{2+} toward various analytes. (D) Fluorescence changes of Coumarin-NH_2-DPA after interaction with different concentrations of Zn^{2+}. (E) Fluorescence intensity of Coumarin-NH_2-DPA-Zn^{2+} toward various analytes. (F) Fluorescence spectra of Coumarin-NH_2-DPA-Zn^{2+} toward various analyte.

The probe complexed with two metal ions separately and observed the effect, the results shown in Figure S3, S4, S5. The probes containing tetraazacycle ring was complexed with copper ions, and the fluorescence showed quenching effect, which almost uncomplexed with zinc ions. The selectivity of Hcy after complexation was good (Figure S3). The fluorescence of the probes containing DPA group were also quenchable when it was complexed with copper ions, but almost all the three biothiols and ATP responded to the probe, and the selectivity was poor. When it was complexed with zinc ions, the fluorescence was enhanced. Almost all the three biothiols and ATP responded to the probe, and the response to ATP was relatively strong (Figure S4 and Figure S5). One of the probes containing DPA, Coumarin-NH_2-DPA, was selected for specific study, and the linear curve of ATP response obtained was shown in the Figure S6A. At the same time, a series of interferences were selected for selective testing, and the results were shown in the Figure S6C. The selectivity of the probe was poor, and it was interfered by various substances. This may

mean that DPA is not a good detection group.

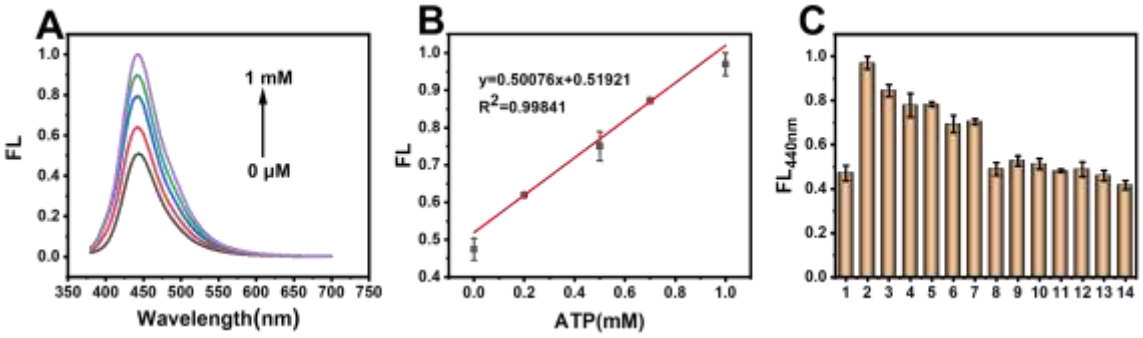

Figure S6. ATP detection with Coumarin-NH_2-DPA-Zn^{2+}. (A) Fluorescence spectra of the probe under different concentrations of ATP: 0, 0.2, 0.5, 0.7, 1 mM. (B) linear calibration curve of fluorescence intensity in Coumarin-NH_2-DPA-Zn^{2+} (10 μM) solution versus concentrations of ATP (0–1 mM). (C) Fluorescence intensity of Coumarin-NH_2-DPA- Zn^{2+} (10 μM) toward various analytes (1. Blank, 2. ATP, 3. ADP, 4. AMP, 5. Hcy, 6. Cys, 7. GSH, 8. Glu, 9. His, 10. Met, 11. Thr, 12. Trp, 13. S^{2-}, 14. SO_3^{2-}).

In addition, to verify the binding ability of NBD-N with copper ions, fluorescence titration experiments were conducted, and the results were provided as Figure S7. As the copper concentration increases, the fluorescence signal of NBD-N decreases. When the copper ions concentration is 10 μM, the fluorescence signal of NBD-N reaches its lowest. It can be obtained that the K_d of NBD-N with copper ions is ~6.03 μM, indicating a good binding ability.

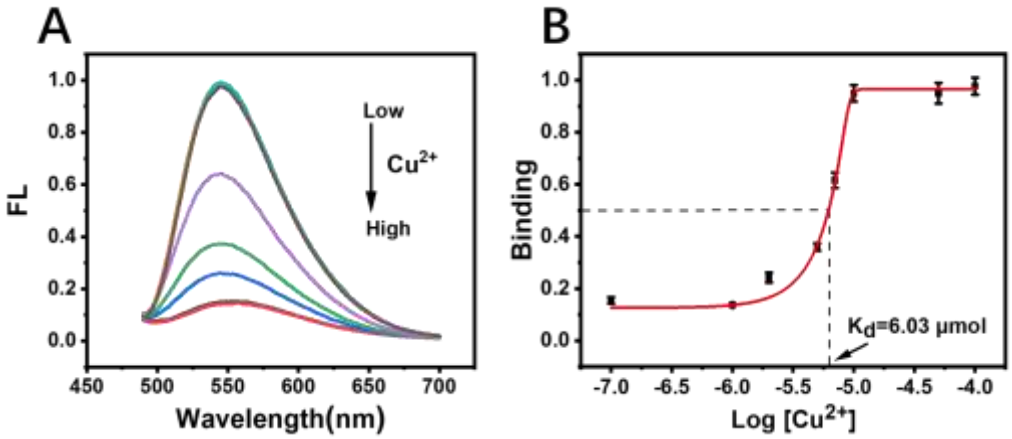

Figure S7. (A) Fluorescence spectra of NBD-N upon addition of varying concentrations of copper ions. (B) Fluorescence titration curves of NBD-N upon treatment with varying concentrations of copper ions.

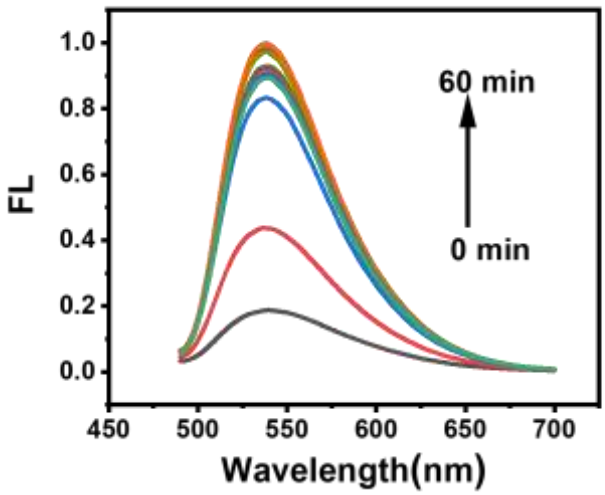

Figure S8. Time-dependent fluorescence changes of NBD-N-Cu^{2+} (10 μM) after the addition of 10 equivalents Hcy.

In order to verify whether free copper ions also have catalytic capabilities, we used the EPR to demonstrate it, as shown in Figure S9. It's observed that free copper ions have obvious characteristic peaks. If free copper ions have catalytic ability, it will be reduced to cupric ions after adding Hcy. However, the EPR results indicated that the copper ions have no valence change during the process after the addition of Hcy. Therefore, it can be concluded that free copper ions have no catalytic effect.

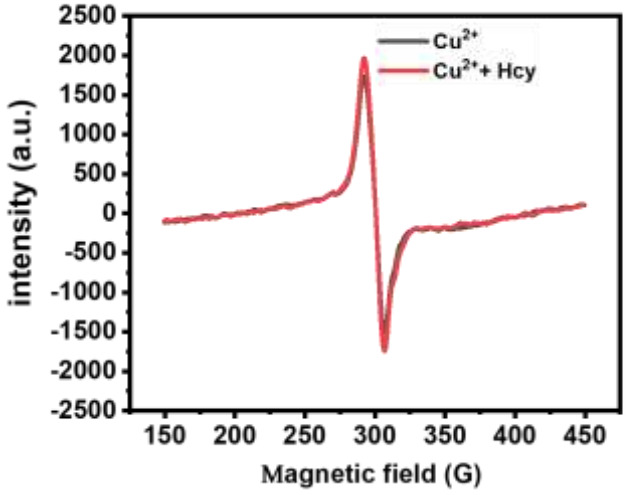

Figure S9. EPR spectra of Cu^{2+} in the absence and presence of Hcy.

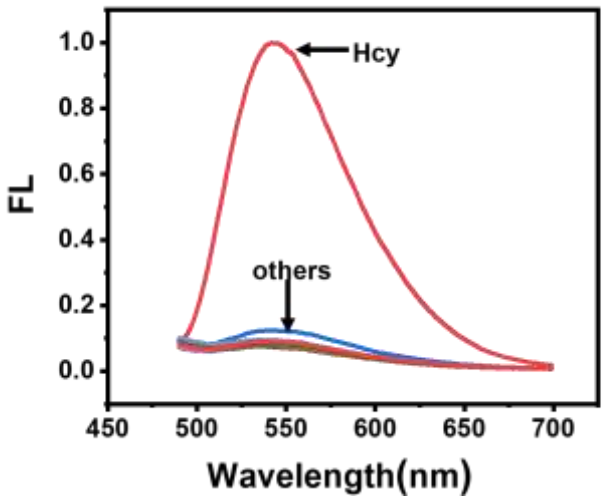

Figure S10. Fluorescence spectra of NBD-N-Cu^{2+} after adding various analytes.

In order to further investigate whether intracellular proteins can strip copper ions, we have supplemented additional experiments that the cell lysate was pretreated with 1 mM N-ethylmaleimide (NEM), a trapping reagent of thiol specie[1]. Then, the sample was analyzed with the NBD-N-Cu^{2+} probe. As shown in Figure S11 (attached below), the fluorescence of the probe was almost unchanged after the addition of the probe, indicating that the intracellular proteins cannot strip copper ions to result in a change in the probe fluorescence. It further evidences the good selectivity of this probe. The above discussion has added into page S9 in Supporting Information.

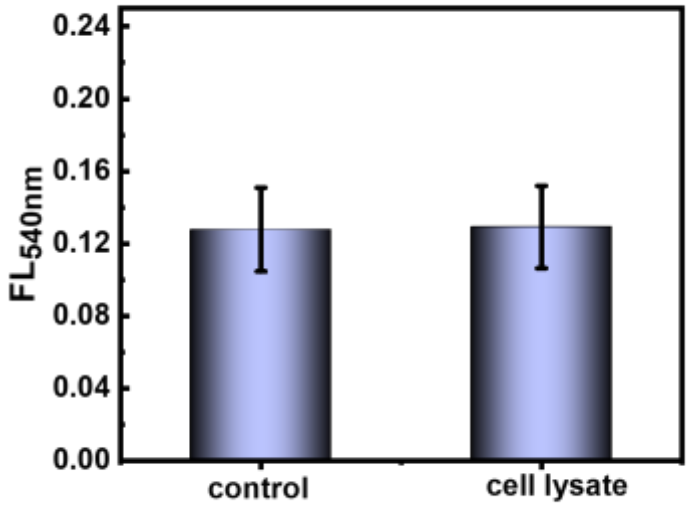

Figure S11. The fluorescence intensity of the probe and its addition to the cell lysate that has already cleared biothiols.

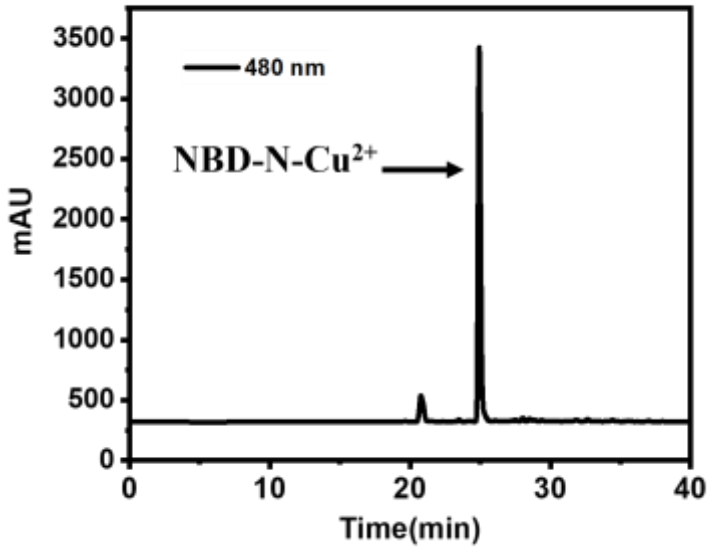

Figure S12. HPLC of NBD-N-Cu^{2+}.

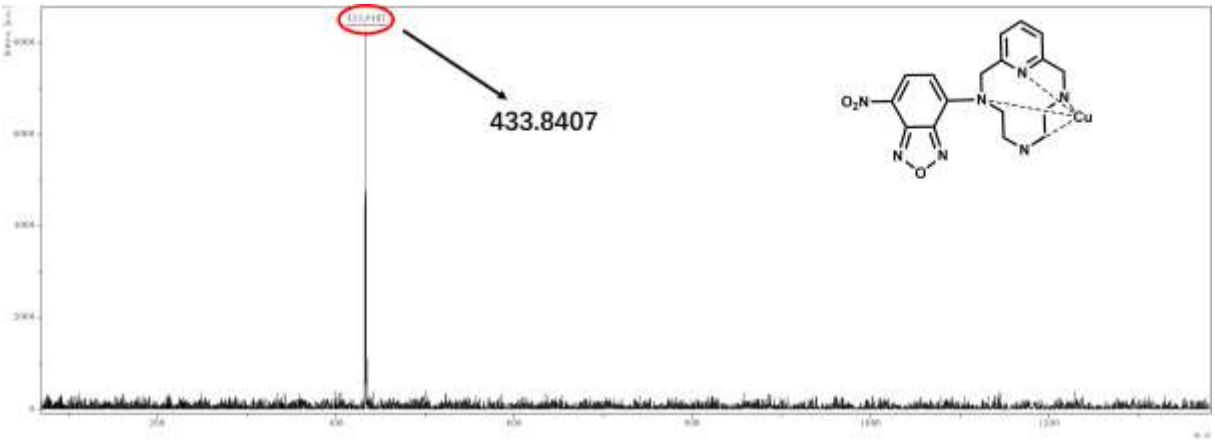

Figure S13. MALDI-TOF-MS of NBD-N-Cu^{2+}.

In order to further explore the stability of the probe, we supplemented its detection ability in PBS, Tris-EDTA, 20% serum, and cell lysate. The results (Figure S14) demonstrated that the probe exhibited equivalent detection capability in all four buffers as in HEPES buffer, which also indicateed that the probe has a good stability and can detect Hcy in various buffer solutions.

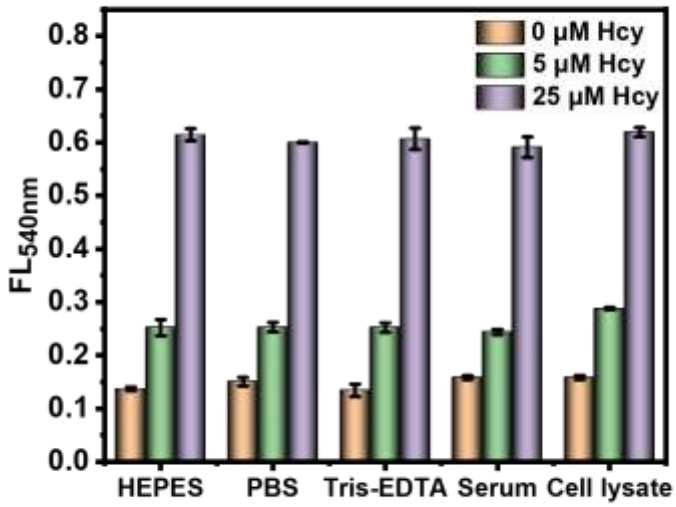

Figure S14. The fluorescence intensity histogram of three different concentrations of Hcy was detected in HEPES, PBS, Tris-EDTA, 20% serum, cell lysate.

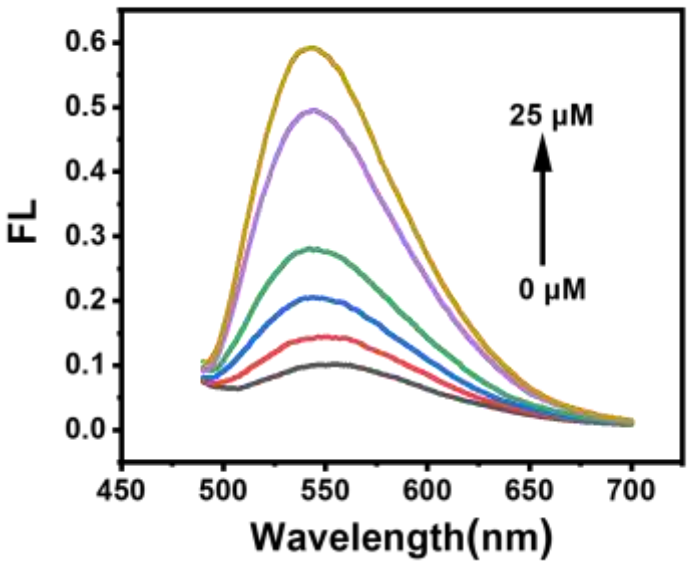

Figure S15. Fluorescence spectra of NBD-N-Cu^{2+} under different concentrations of Hcy in human serum:

0, 2, 5, 10, and 25μM.

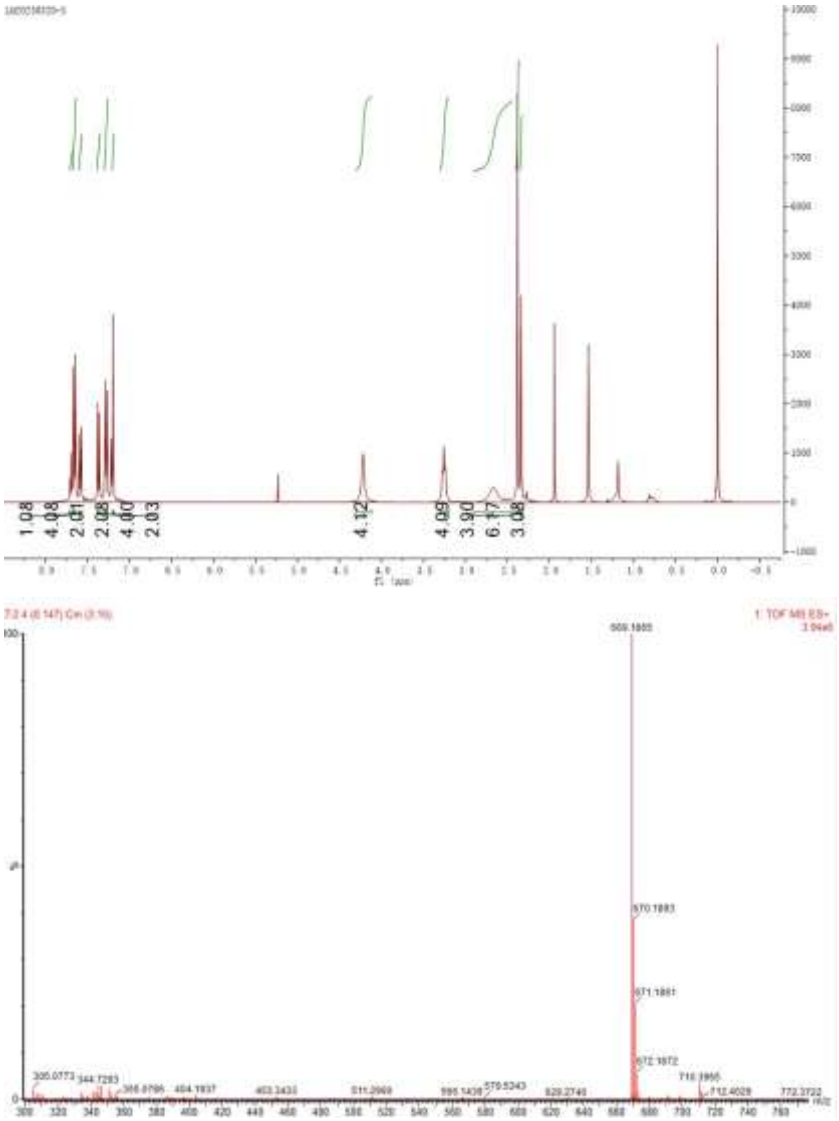

Figure S16. ^{1}H NMR and MS spectrum of $PyNTs_3$.

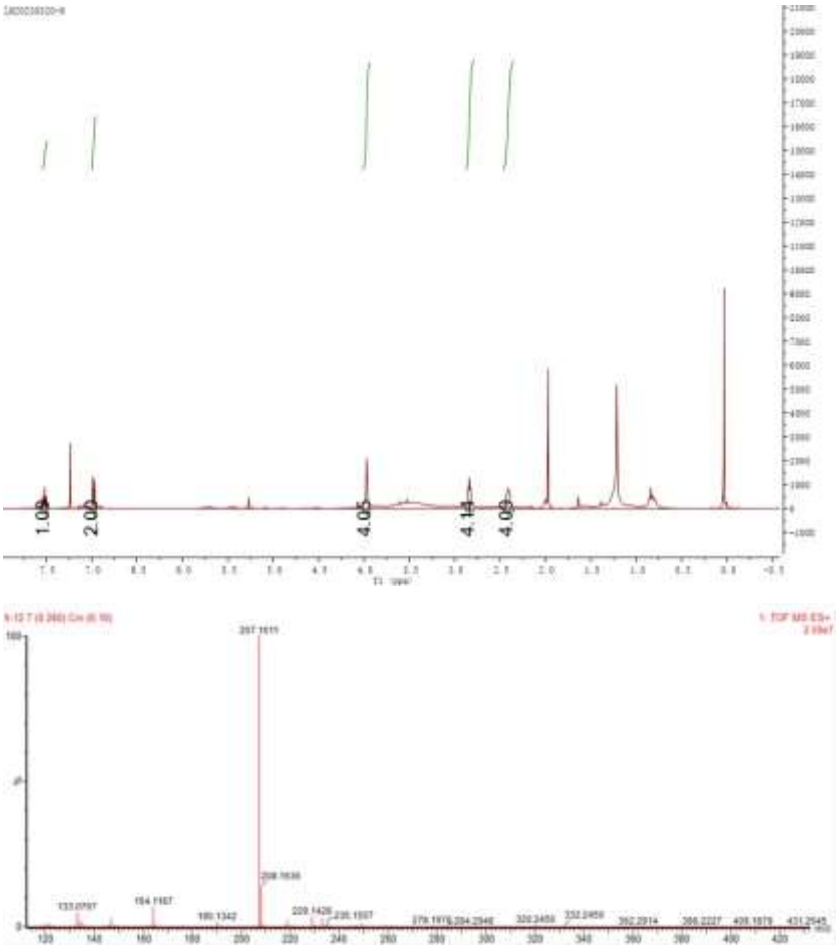

Figure S17. ^{1}H NMR and MS spectrum of $PyNH_3$.

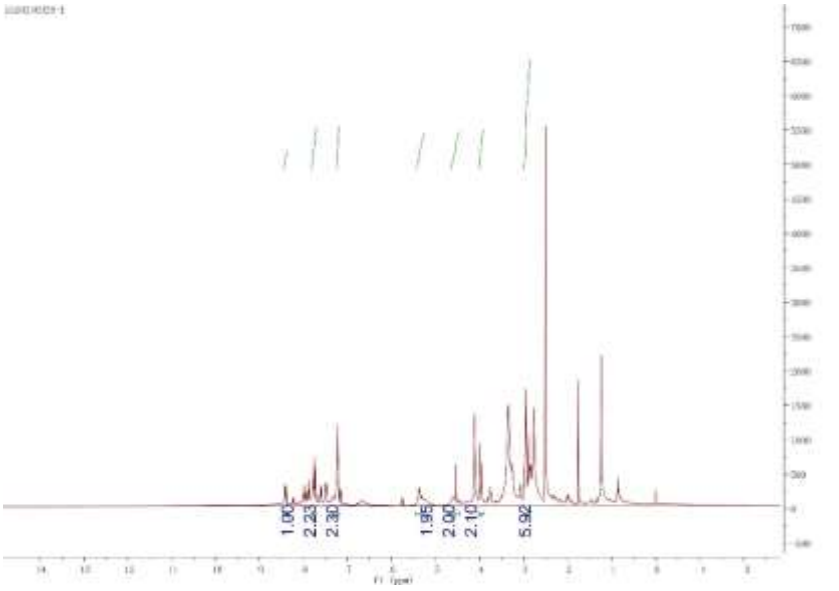

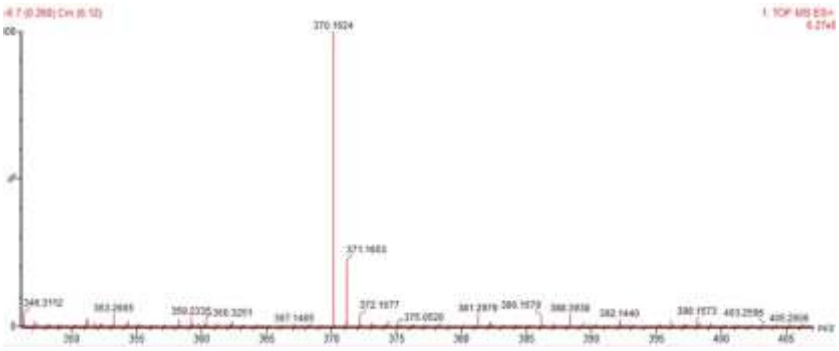

Figure S18. [1]H NMR and MS spectrum of NBD-N.

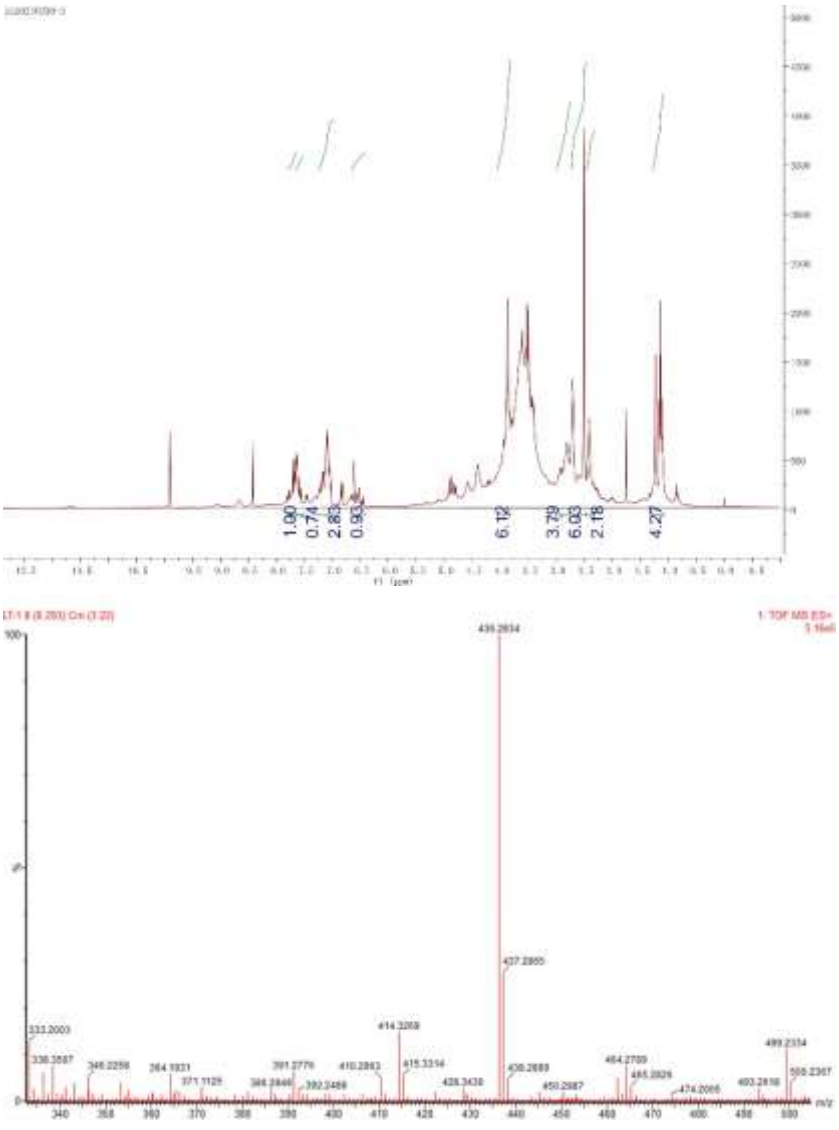

Figure S19. [1]H NMR and MS spectrum of Coumarin-N.

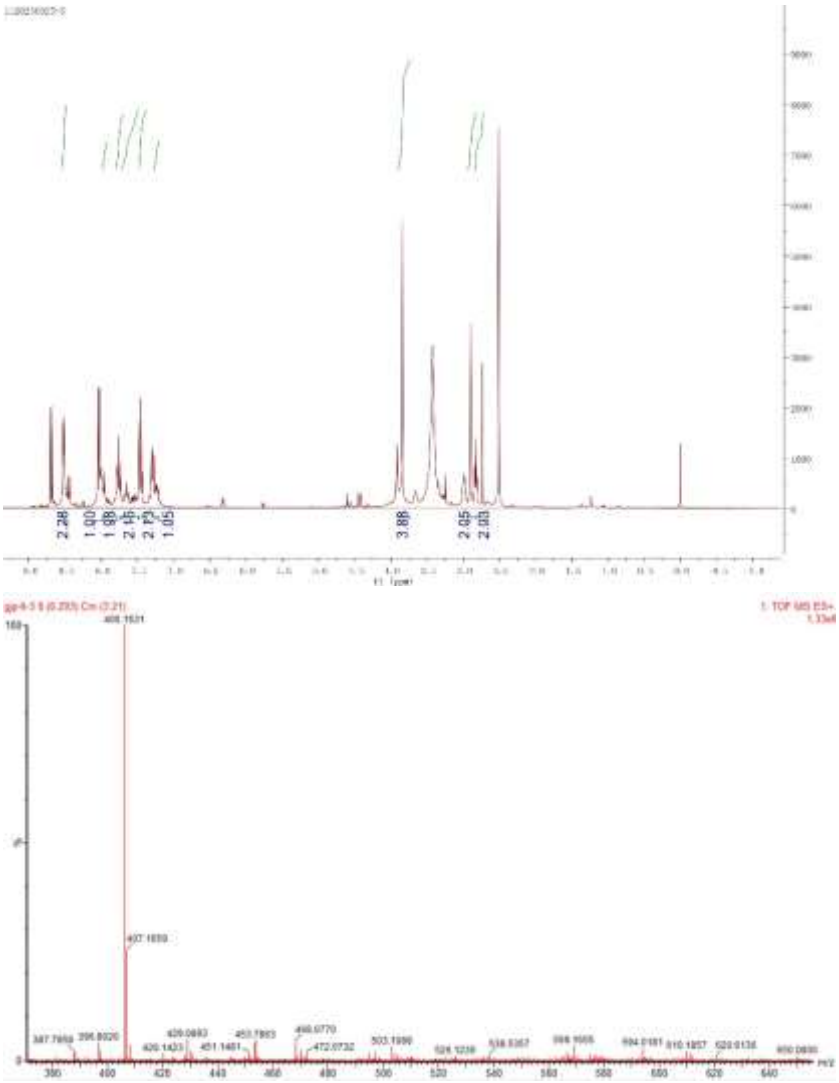

Figure S20. ^{1}H NMR and MS spectrum of NBD-NH_2-DPA.

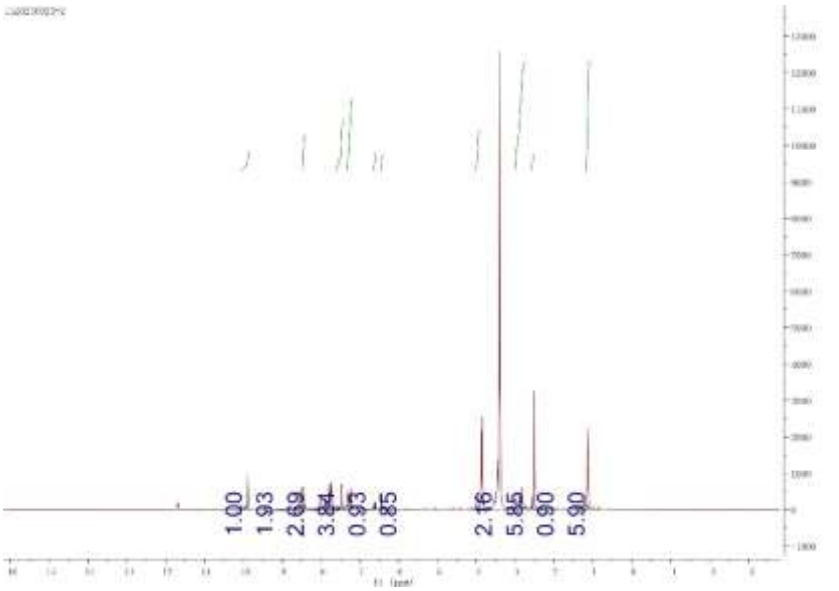

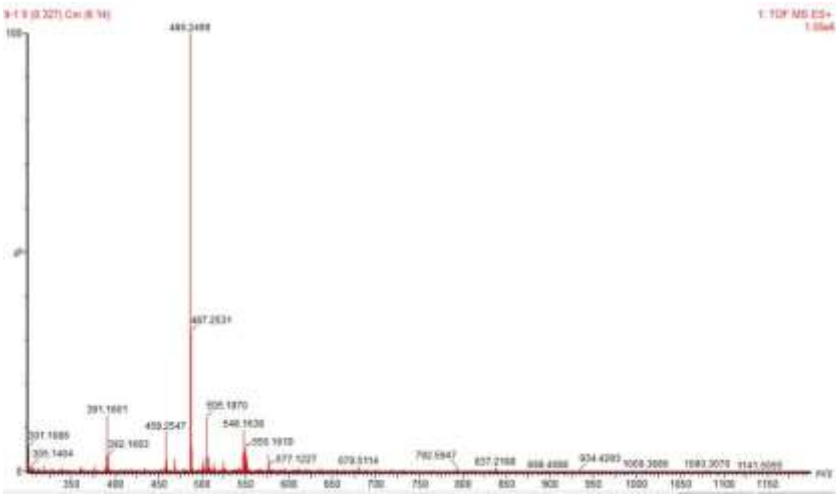

Figure S21. ^{1}H NMR and MS spectrum of Coumarin-NH_2-DPA.

[1]. Liu, J.; Sun, Y.-Q.; Zhang, H.; Huo, Y.; Shi, Y.; Guo, W., Simultaneous fluorescent imaging of Cys/Hcy and GSH from different emission channels. *Chem. Sci.* **2014,** *5* (8), 3183.